Catalysis Science & Technology

PAPER

View Article Online
View Journal | View Issue

Cite this: *Catal. Sci. Technol.*, 2019, **9**, 6638

Novel metallic electrically heated monolithic catalysts towards VOC combustion†

Qiulian Zhu,[a] Hao Li,[a] Yue Wang,[a] Ying Zhou,[a] Anming Zhu,[a] Xiao Chen,[ab] Xiaonian Li,[a] Yinfei Chen[a] and Hanfeng Lu *[a]

Received 25th July 2019,
Accepted 7th October 2019

DOI: 10.1039/c9cy01477b

rsc.li/catalysis

The development of metallic monolithic catalysts with various morphologies to catalyze rapid combustion of volatile organic compounds (VOCs) under high space velocity is a profound challenge in catalyst research. Herein, we reported the preparation of novel electrically heated monolithic Pt and Pd catalysts supported on an FeCrAl metal wire. The catalysts exhibited high catalytic activity for the VOC combustion to CO_2 and H_2O under low-current DC power. Notably, the catalysts exhibited nearly 100% toluene and ethyl acetate conversion rates under a DC power of 5 W and 8 W and a space velocity of 30 000 mL h^{-1} g^{-1} with a combustion response time of less than 30 s. The exceptional activity of the catalysts can be attributed to a well-adhered alumina coating that formed on the surface of the FeCrAl metallic substrate after thermal treatment and highly dispersed Pt and Pd nanoparticles on the surface of an alumina coating. Meanwhile, surface temperature can instantly reach the desired ignition point, because of high thermal conductivity and electrical conductivity.

1 Introduction

In recent years, gaseous pollutant emissions caused by rapid urbanization and industrialization have become increasingly worse, and volatile organic compounds (VOCs) are recognized as major contributors to air pollution.[1–11] Catalytic combustion is one of the most effective and economically feasible technologies for VOC removal.[12–19] Monolithic catalysts, which are commonly composed of ceramic or metal materials, are widely used in catalytic combustion because of their excellent attrition and low pressure drop even at a high flow rate.[20–23] Metallic materials exhibit higher thermal conductivity and mechanical resistance, better electrical conductivity, and lower manufacturing costs than ceramic materials.[21,24,25] Therefore, the application of metallic substrates as catalyst supports has become more and more common.[26–29] Metallic monolithic catalysts are prepared through steam-only oxidation,[30] anodization,[31] or electrophoretic deposition.[32] Cimino *et al.* prepared a catalyst for methanol oxidation through the cathodic electrodeposition of Pt onto commercial 50 ppi FeCr alloy foams. They controlled the Pt deposition by varying electrical charges. The Pt–FeCr alloy foams exhibited 100% CO_2 conversion, excellent stability and reusability, and low CO emissions.[33]

As we all know, regenerative thermal oxidation (RTO) and regenerative catalytic oxidation (RCO) are the two main treatment technologies for VOC pollution control.[34,35] However, these traditional technologies usually require an external heat source, such as a heating furnace to heat the catalysts bed.[36–39] This requirement extends combustion response time and slows initial combustion rates. In addition, several important issues remain unresolved in the fabrication of metal-supported catalysts for VOC combustion, including: (1) the process complexity and poor adhesion of conventional wash-coating methods;[40–43] (2) the limitation of active component loading due to carrier shape; (3) the existence of an unstable state that results in VOC emission. Therefore, metallic monolithic catalysts prepared by a simple and general method, with a solid and well-adhered coating, changeable shape, and fast response to changing conditions, are highly desired for rapid VOC combustion under high space velocity.

Here, we report novel electrically heated monolithic Pt Pd catalysts supported on FeCrAl metal wires and fabricated through a simple strategy. Active noble metal nanoparticles (NPs) in liquid *n*-hexane were synthesized by a solvothermal method (Fig. 1), and spraying carriers with dispersion liquid was used to randomly load active species. Pt and Pd NPs were highly dispersed on the surface of a metallic substrate with a monomolecular membrane and were firmly bonded to a

[a] *Innovation team of air pollution control, Institute of Catalytic Reaction Engineering, College of Chemical Engineering, Zhejiang University of Technology, Hangzhou 310014, China. E-mail: luhf@zjut.edu.cn; Tel: +86 571 88320767*
[b] *Institute of Environmental Chemicals and Resources, College of environment, Zhejiang University of Technology, Hangzhou 310014, China*

† Electronic supplementary information (ESI) available. See DOI: 10.1039/c9cy01477b

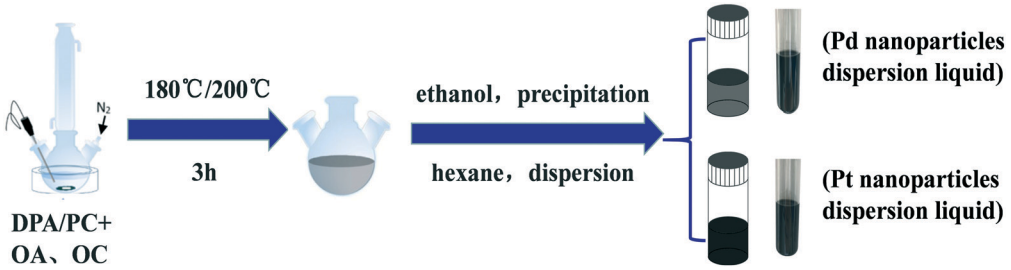

Fig. 1 Preparation of Pt and Pd nanoparticle (NP) dispersion liquids (DPA: dinitrodiammineplatinum ammoniacal, PC: palladium chloride, OA: oleylamine, OC: oleic acid).

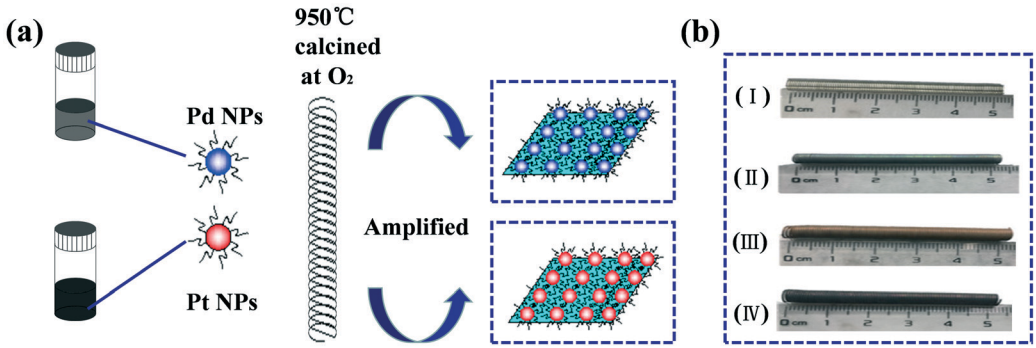

Fig. 2 (a) The scheme of the preparation of Pt and Pd monolithic catalysts; (b) photographs of (I) the untreated FeCrAl metallic monolith, (II) FeCrAl metallic monolith calcined at 950 °C for 3 h under O_2 atmosphere, (III) FeCrAl metallic monolith loaded with Pd NPs and (IV) FeCrAl metallic monolith loaded with Pt NPs.

metallic substrate after calcination (Fig. 2a and b). The metallic substrate was utilized because of its excellent electrical conductivity, which can be self-heated electrically and rapidly through direct connection to a DC power supply.

2 Experimental

2.1 Preparation of the electrically heated metallic monolithic catalysts

34.6 mg DPA (or 35.2 mg PC) was mixed with 3 mL OA and 2 mL OC (or 6 mL OA and 2 mL OC) in a three-necked flask equipped with a condenser and a stir bar, followed by heating and maintained at elevated temperatures (200 °C for Pt, 180 °C for Pd) for 3 h under flowing N_2 atmosphere. Subsequently, the particles thus formed were purified by precipitation in triple volumes of ethanol, centrifuged (6000 rpm, 5 min), washed twice with 10 mL ethanol, and redispersed in 10 mL *n*-hexane. The FeCrAl metallic wire (0.50 mm in diameter) was utilized as the substrate and machined into a spiral shape. Then, the FeCrAl metallic substrate was immersed in acetone, 10 wt% NaOH and 10 wt% HNO_3 with ultrasonic treatment for 30 min. Subsequently, the FeCrAl metallic substrate was calcined in O_2 atmosphere at 950 °C for 3 h. A ready-made Pt and Pd nanoparticle dispersion liquid were supported on the FeCrAl metallic substrate by spraying, then, the monolithic catalysts were dried at 110 °C for 2 h and calcined at 500 °C for 5 h. The loading of Pt and Pd is 0.1 wt% (it refers to the theoretical value), and the monolithic catalysts are denoted 0.1Pt/FeCrAl and 0.1Pd/FeCrAl.

2.2 Characterization

The SEM images and EDS results were taken using a Hitachi-SU8010 SEM with an acceleration voltage of 5 kV for imaging and 15 kV for EDS collection. The TEM images were taken on a Tecnai G2 F30 S-Twin (Philips-FEI, Netherlands) transmission electron microscope at an acceleration voltage of 200 kV. The samples were dispersed in ethanol assisted by an ultrasonic technique. The adhesion of the samples was evaluated using ultrasound (KH3200E, Kunshan Hechuang Ultrasonic Instrument Co. Ltd.) tests by immersing the samples in water with ultrasound for 1 h. After the samples were dried at 110 °C for 2 h and calcined at 500 °C for 2 h, the weight loss was measured.

The X-ray photoelectron spectra were taken using monochromatized Al Kα irradiation a Thermo Escalab 250Xi. The samples were cut into 5 mm in length and sonicated in anhydrous ethanol for 20 min, then mounted onto the double-sided adhesive tape on a sample holder. All binding energies (BEs) were referenced to the C 1s peak (284.8 eV).

2.3 Catalytic performance test of the electrically heated metallic monolithic catalysts

VOC catalytic combustion measurement was conducted with a fixed-bed continuous flow reactor. The Pt and Pd

monolithic catalysts (about 2.0 g) were carefully held in a 6 mm (i. d.) quartz tubular reactor, while a K-type thermocouple was placed in the region of the catalyst bed to monitor the reaction temperature. The monolithic catalysts were connected to a DC power supply (HSPY-60-02, Beijing Hanshengpuyuan Technology Co. Ltd.) using wires. The concentration of VOCs was 2500 ppm, balanced with air, and the total flow rate was controlled with a mass flow controller. The concentration of the VOCs at the outlet was monitored with a gas chromatograph (Kexiao, GC1620) equipped with a flame ionization detector (FID). The concentration of the oxidative product (CO_2) was monitored with a mass spectrometer (MKS Cirrus 2). The percent conversions were the values calculated according to the equation: % conversion = {[VOCs]in − [VOCs]out}/[VOCs]in × 100%, where [VOCs]in and [VOCs]out represent the concentrations of the VOCs at the inlet and outlet, respectively. The concentrations of the feed and output gases correspond to the peak areas.

3 Results and discussion

The transmission electron microscopy (TEM) images of the Pt and Pd NPs are shown in Fig. 3. The Pt and Pd NPs are quasi-spherical in shape and nearly monodispersed with low aggregation and a narrow size distribution.[44–47] Moreover, the size histograms show that the average sizes of the Pt NPs are in the range of 2–4 nm and the Pd NPs are in the range of 2–5 nm. The extensive dispersion of Pt and Pd NPs on the surfaces of the metallic substrate can be attributed to their monodispersed structure.[48] The active noble metal NPs can be randomly loaded on the metallic substrate through spraying given that they are scattered in *n*-hexane in liquid form. It deserves to be mentioned that loading by spraying is not limited by carrier morphology.

To promote the anchorage of the coating to the metallic substrate,[42] the FeCrAl substrate was thermally treated at 950 °C for 3 h under O_2 atmosphere. In order to confirm if the applied treatments resulted in the formation of a uniformly roughened surface on the metallic substrate, the morphology and composition of the FeCrAl substrate and monolithic catalysts were investigated.[26] The scanning electron microscopy (SEM) micrographs and energy-dispersive X-ray spectroscopy (X-EDS) results of the FeCrAl substrate surfaces are shown in Fig. 4. The SEM micrographs of untreated FeCrAl metallic substrate are shown in Fig. 4a. The FeCrAl metallic substrate exhibited slightly cracked smooth surfaces. The SEM micrographs of the FeCrAl metallic substrate calcined at 950 °C for 3 h are shown in Fig. 4b which show the generation of uniformly roughened surfaces. Bulk aluminum has a higher chemical potential and is more likely to undergo an oxidation reaction with oxygen, so it can easily migrate from the bulk to the surface and reacts with oxygen to form alumina whiskers.[49,50] These structures promote the firm bonding of the active phase to the metallic substrate. EDS mapping analysis shows that the Al and O atoms are distributed over the entire field with similar dispersions. The SEM micrographs of the monolithic catalysts are presented in Fig. 4c and d, which allow us to appreciate the formation of a homogeneous surface by the Pt and Pd catalysts on the whiskers or pores. The EDS mapping of Pt and Pd indicates that the Pt and Pd NPs are highly dispersed on the alumina coating. In preparing monolithic catalysts, the adherence of coatings and active phases to metallic substrates is crucial. The adhesion of the wash-coating and active components was evaluated through ultrasound tests. Considering the margin of the experimental error, the catalysts have no obvious weight loss after ultrasound treatment, indicating the excellent adhesion of the alumina coating and active species to the FeCrAl metallic substrate surface (see ESI† Table S1).

The elemental compositions of the FeCrAl monoliths are presented in Table 1, and the EDS spectra of the monoliths are shown in the ESI† Fig. S1. The elemental composition of the FeCrAl metallic substrate was elucidated through EDS,

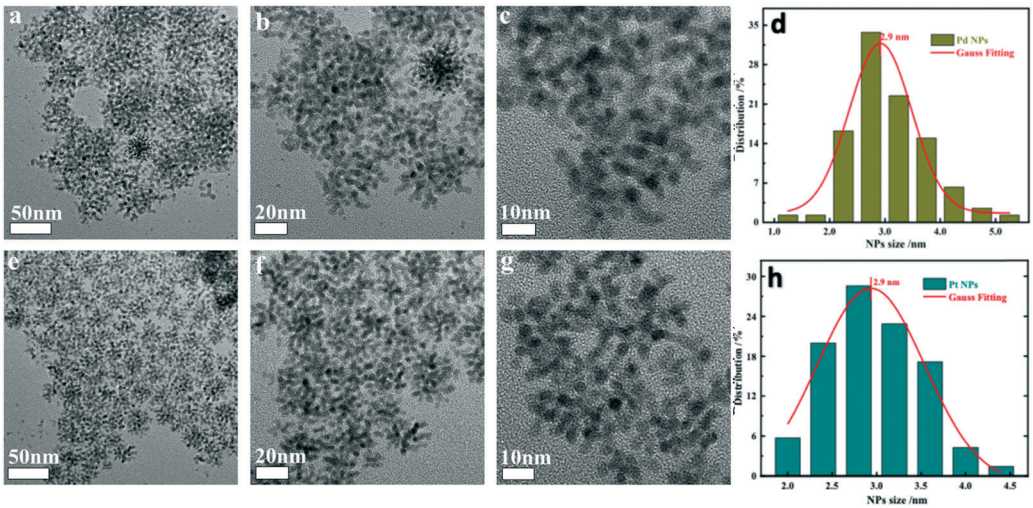

Fig. 3 TEM images of Pd (a–c) and Pt (e–g) NPs and their corresponding size histograms (d and h).

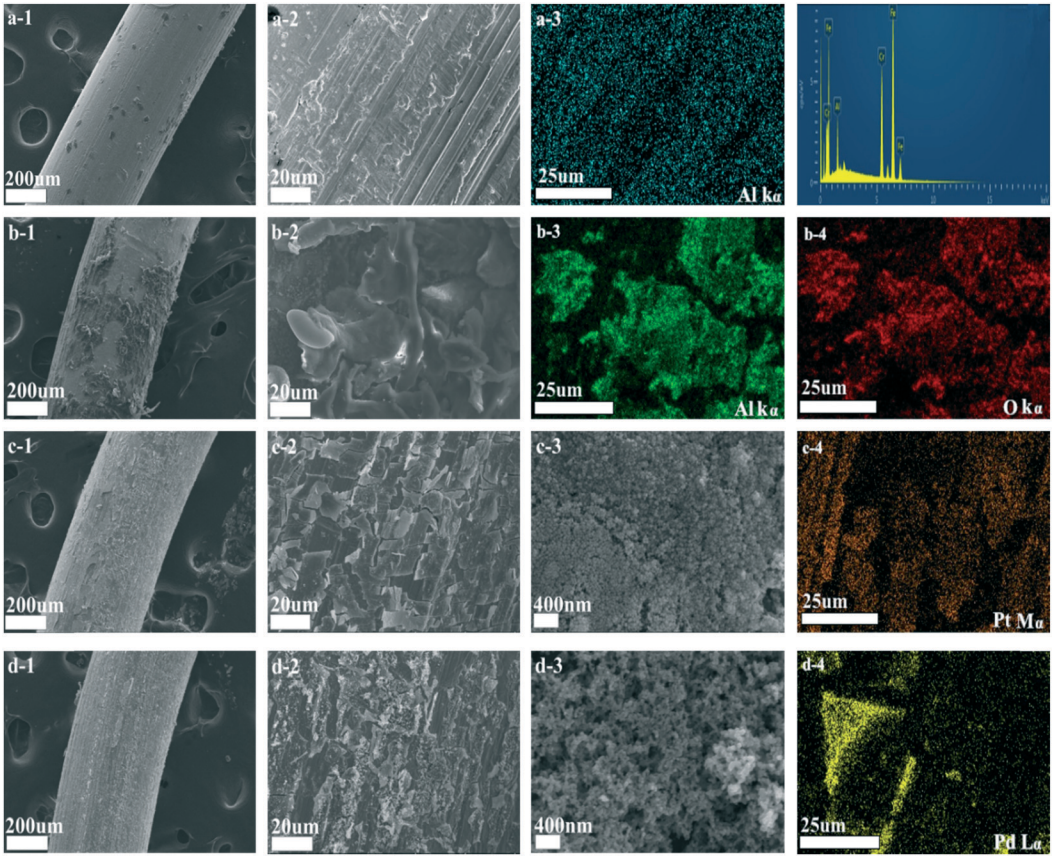

Fig. 4 SEM and mapping images (EDS results) of the FeCrAl monoliths. (a) FeCrAl; (b) calcined FeCrAl; (c) 0.1Pt/FeCrAl; (d) 0.1Pd/FeCrAl.

which reports the mass percentages of each chemical element (Fe, Cr and Al) with values similar to those reported by the manufacturers listed in the materials. The EDS analysis of the FeCrAl substrate after thermal treatment (950 °C for 3 h under O_2 atmosphere) indicates that the elemental composition on the FeCrAl substrate surface has changed. Specifically, the percentages of Al and O increases, whereas that of Fe decreases because of the formation of alumina.[51,52] Thus, the well-adhered alumina coating can firmly bond the noble metal NPs to the FeCrAl substrate. The EDS analysis of Pt and Pd indicates that the active phase bonds with the metal substrate and the thermal treatment increases the exposed area of the FeCrAl substrate, which makes the nanoparticles more evenly dispersed. The adherence of the active phase with the metal substrate ensures catalytic activity.

Table 1 Atomic composition of the FeCrAl monoliths as determined through X-EDS

Sample	Element	Weight/%	Atomic/%
FeCrAl	Al	3.87	7.68
	Cr	25.24	25.56
	Fe	70.88	66.76
Calcined FeCrAl	O	11.56	26.43
	Al	20.16	27.33
	Cr	31.32	22.03
	Fe	49.96	24.21
0.1Pt/FeCrAl	O	14.41	34.21
	Al	19.93	28.04
	Cr	15.95	11.65
	Fe	33.84	23.01
	Pt	15.88	3.09
0.1Pd/FeCrAl	O	15.91	36.42
	Al	13.80	18.73
	Cr	19.43	13.68
	Fe	43.88	28.77
	Pd	6.98	2.40

Metallic substrates have excellent electrical conductivity. Joule's law states that a metallic substrate will rapidly self-heat when connected to a DC power supply. To investigate the heating performance of the FeCrAl substrate, the metallic monoliths were directly connected to a DC power supply and the surface temperatures were measured using thermocouples (Fig. 6a). As shown in Fig. 6b, when the temperature approaches 300 °C under a current of 1.2 A , VOC catalytic combustion seems to occur, while the temperature of the FeCrAl substrate rapidly increases to 300 °C within 30 s. By contrast, the temperature of the FeCrAl substrate quickly decreases when the power is turned off. This phenomenon can be attributed to the favourable thermal and electric conductivities of the metallic substrate. Therefore, the rapid catalytic combustion of VOCs can be achieved under low power input. In addition, exterior-to-

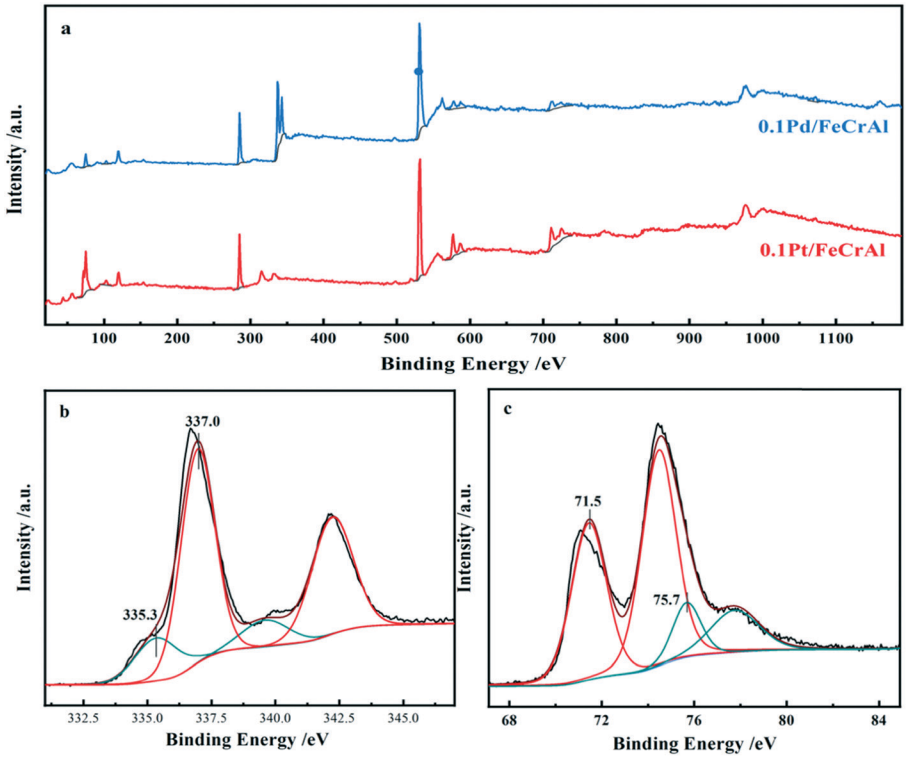

Fig. 5 The photoemission spectra recorded for (a) 0.1Pd/FeCrAl and 0.1Pt/FeCrAl; (b) Pd 3d; (c) Pt 4f.

interior heat transfer shortens the response time of catalytic combustion.

The XPS spectra of the Pd/FeCrAl and Pt/FeCrAl catalysts are shown in Fig. 5a–c, and all the spectra are presented by subtraction of the Shirley background from experimental spectra. As shown in Fig. 5b, there are two states of Pd species on the Pd/FeCrAl catalysts with Pd $3d_{5/2}$ binding energy (BE) values of 335.3 eV and 337.0 eV, respectively. The Pd species with a BE of 337.0 eV could be attributed to the species Pd^{2+} in the form of PdO on the surface of the Pd/FeCrAl catalyst[53] and the peak at 335.3 eV could be induced by Pd^0 on the surface.[54] These results suggest that more Pd species are in the form of Pd^{2+} rather than Pd^0. As shown in Fig. 5c, there are two states of Pt species on the Pt/FeCrAl catalysts with Pt $4f_{7/2}$ binding energy (BE) values of 71.5 eV and 75.7 eV, respectively. The Pt species with a BE of 71.5 eV could be attributed to the species Pt^0 (ref. 55) and the peak at 75.7 eV could be induced by Pt^{4+} in the form of PtO_2 on the surface.[56] The higher BE indicates that more electrons transfer from Pt to the MO_x coating due to the intensified interaction between them.[55]

To demonstrate the catalytic activity of the electrically heated catalysts, the catalytic combustion of toluene and ethyl acetate over Pt- or Pd-loaded monoliths was investigated. As shown in Fig. 6d, blank FeCrAl monoliths exhibited low toluene conversion rates below 12 W. These results suggest that the FeCrAl monoliths do not exhibit considerable toluene combustion activity; direct thermal oxidation of toluene in the absence of the active species is negligible under test conditions.[57] By contrast, the 0.1Pt/FeCrAl and 0.1Pd/FeCrAl catalysts exhibited excellent toluene combustion conversion of 100% under 5 W. The products of the toluene combustion reaction were analysed by GC and MS (see ESI† Fig. S2). This result, in addition with SEM and TEM observations, indicates that the catalytic activity is improved by the formation of a well-adhered alumina coating on the surfaces of the FeCrAl metallic substrate through thermal treatment and the high dispersion of Pt and Pd NPs on the surfaces of the alumina coating. Pd^0 (or Pt^0) is initially oxidized by O_2 to form very active $[Pd^{2+}O^{2-}]$ (or $[Pt^{2+}O^2]$) species and a Pd^{2+} (or Pt^{2+}) cation is simultaneously reduced to Pd^0 (or Pt^0) as toluene is oxidized to CO_2 and H_2O over active $[Pd^{2+}O^{2-}]$ (or $[Pt^{2+}O^2]$) species.[58] In addition, the mass spectroscopy (MS) results (Fig. 6e and f) show that carbon dioxide emission is satisfactory. The ignition curve can be represented by either a VOC decline curve or a CO_2 rising curve.[25] These results collectively indicate that the catalysts exhibit high CO_2 selectivity. Furthermore, the catalytic combustion rapidly occurs with a response time of less than 30 s. The catalytic combustion of toluene is quickly completed under DC power and terminated as the DC power is turned off. This on–off reaction model is suitable for industrial VOC control because of its unstable emissions. The activity of the catalysts for ethyl acetate combustion (Fig. 6g) is inferior to that for toluene combustion. Nevertheless, the catalysts exhibited 98% ethyl acetate conversion under 8 W within 1 min, and the products of the combustion reaction are analysed by GC and MS (see ESI†

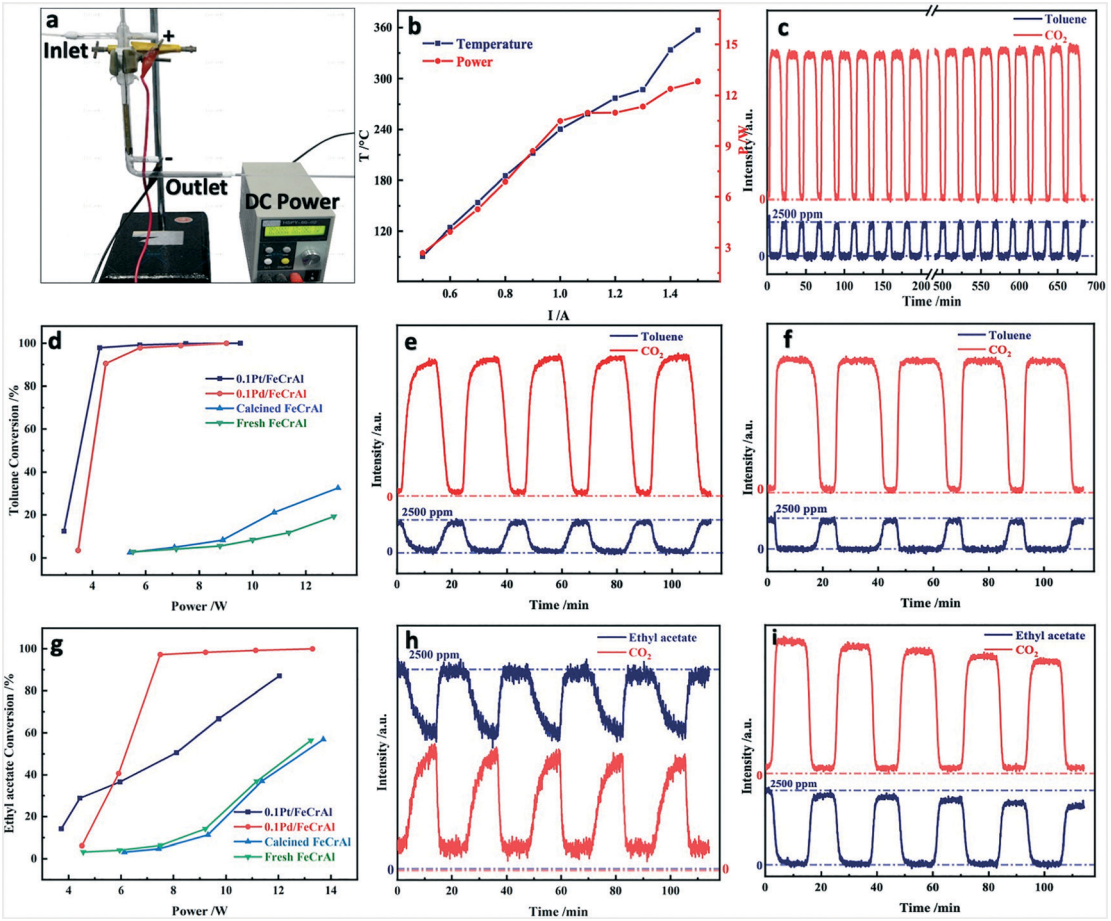

Fig. 6 (a) Image of the electrically heated metallic monolithic catalyst reactor; (b) heating performance of the FeCrAl substrate; (c) stability of 0.1Pd/FeCrAl in toluene combustion (I = 0.9 A); (d) light-off curves of toluene catalytic combustion and MS tested curves of toluene catalytic combustion (I = 0.9 A) over (e) 0.1Pt/FeCrAl and (f) 0.1Pd/FeCrAl; (g) light-off curves of ethyl acetate catalytic combustion and MS tested curves of ethyl acetate catalytic combustion (I = 1.0 A) over (h) 0.1Pt/FeCrAl and (i) 0.1Pd/FeCrAl. Other conditions: toluene and ethyl acetate concentrations of 2500 ppm and WHSV of 10 000 mL h^{-1} g^{-1}.

Fig. S3). The catalytic combustion of ethyl acetate is more difficult to achieve than that of aromatic compounds.[7,59,60] Interestingly, in good agreement with the MS results, 0.1Pd/FeCrAl exhibits better catalytic activity than 0.1Pt/FeCrAl (Fig. 6h and i). Ethyl acetate oxidation reactions over Pd/Al_2O_3 and Pt/Al_2O_3 are found to be structure sensitive reactions, and in most probability, ethyl acetate decomposes to ethanol and acetic acid.[61,62] Furthermore, this result implies that the catalytic activity may be related to the interaction between the active compound and the support. Additionally, the catalysts exhibit excellent performance in the catalytic combustion of other VOCs (see ESI† Fig. S4). We can conclude that the order of the catalytic activities of our catalysts for the VOC combustion is oxygenated (nitrogen) > chain alkane compounds, because the molecular structure of chain alkanes is extremely stable and difficult to be oxidized. In summary, the Pt and Pt catalysts exhibit superior performance for the VOC catalytic combustion. In addition, we have listed a comparison with other systems in the literature (see ESI† Table S2). To examine the stability of 0.1Pd/FeCrAl, additional experiments were conducted for 30 cycles under 10 000 mL h^{-1} g^{-1} space velocity, 2500 ppm toluene concentration, and 0.9 A power current. As shown in Fig. 6c, excellent catalytic activities are observed during these cycles. After 30 cycles, the catalyst still has a conversion rate of 100%. These results suggested that our catalysts have excellent stability and can be applied in the industrial combustion of VOCs. The reusability of the catalysts shows that 0.1Pd/FeCrAl worked well for at least 10 runs without significant activity loss (see ESI† Fig. S5).

The effect of WHSV on catalytic performance was investigated, and the light-off curves of the catalysts are shown in the ESI† Fig. S6. Obviously, increased WHSV leads to a lower toluene conversion under the same reaction temperature, which may be caused by the shorter residence time of toluene in the catalyst bed under higher WHSV. Nevertheless, the catalysts exhibit excellent activities under high space velocity. These can be attributed to the rapid response rate of the catalysts, since the reactant molecules (O_2 and toluene) diffuse to the surface of the metallic monolithic catalysts at high temperature, thereby favouring oxidation reactions going to completion.[63] These results

demonstrate that the Pt- and Pd-loaded monoliths can be used to catalyse the combustion of high-flux VOCs. Therefore, our Pt- and Pd-loaded monoliths have potential industrial applications. Moreover, we also studied the effect of noble metal loading on the catalytic activity for toluene combustion (see ESI† Fig. S7). From an economic point of view, a highly active catalyst with a low palladium component is desirable. Obviously, the lower the Pd loading, the lower the catalytic activity, because the metal loading has a direct effect on the quantity of the active components. Lower Pd loading leads to less distribution on the surface of the FeCrAl metallic substrate, resulting in less active sites and worse catalytic activity. When the Pd loading is 0.1 wt%, and the Pd NPs can be completely dispersed on the FeCrAl metallic substrate, therefore, the 0.1Pd/FeCrAl catalyst exhibits superior activity for toluene combustion. Thus, this highly active catalyst with a low Pd loading has broad prospective industrial applications.[64]

To further study the potential industrial applications of the electrically heated monolithic catalysts, we performed an amplifying experiment. As shown in Fig. 7a, toluene was diluted with air to a desired concentration and transported using an air pump into a quartz fixed reactor charged with the 0.1Pd/FeCrAl catalyst. The images shown in Fig. 7d reveal that toluene is rapidly degraded.

When the current is switched to 1.4 A under a power of 414 W, the temperature of off-gas reaches approximately 300 °C and the toluene conversion reaches 90%, at 15.4 × 104 h^{-1} space velocity and 2500 ppm toluene concentration. Furthermore, when the current is switched to 1.4 A under a power of 433 W at a space velocity of 11.34 × 104 h^{-1}, the toluene conversion reaches 98% (Fig. 7e), which indicates

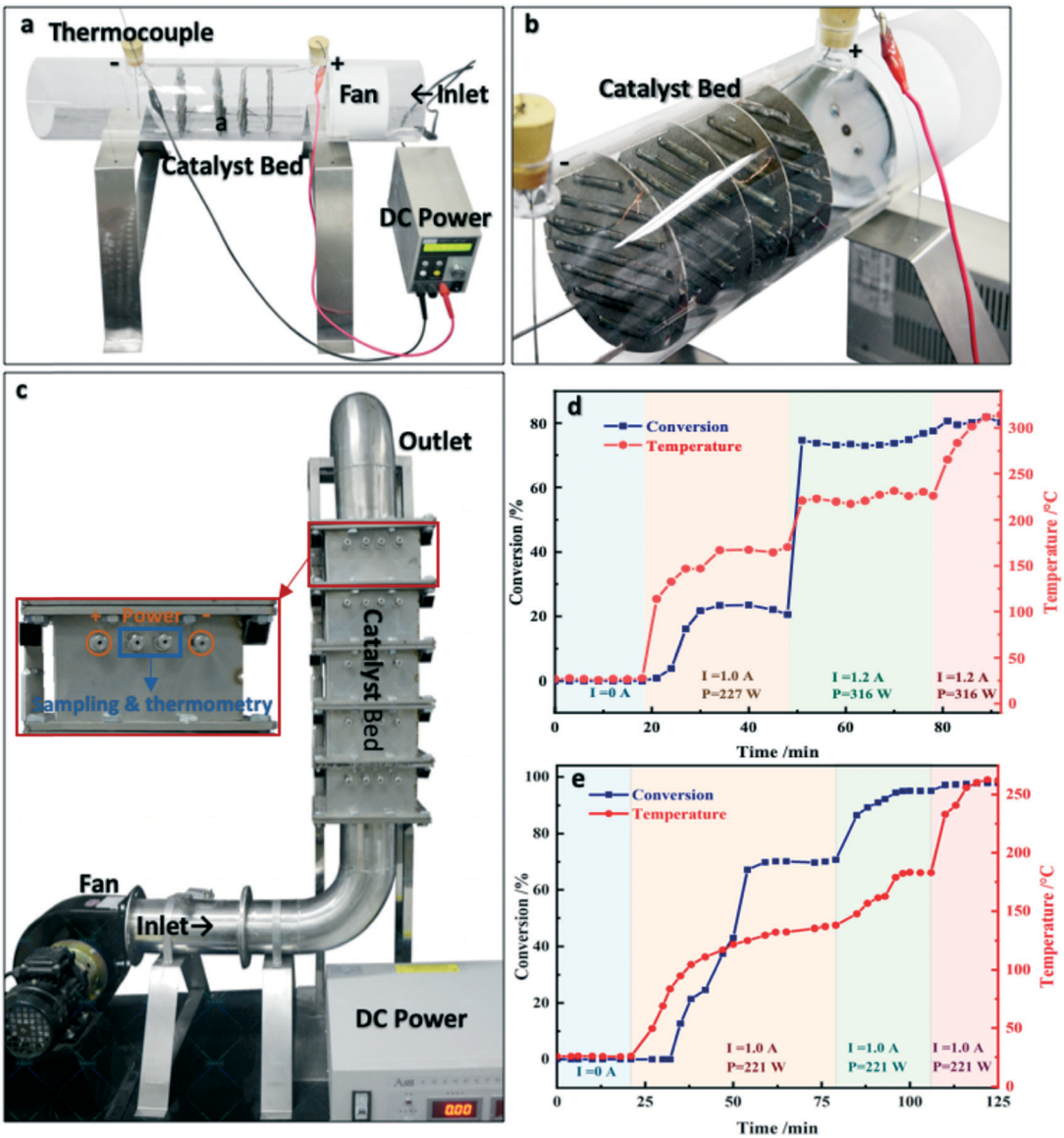

Fig. 7 (a and b) Images of the amplifying experiment apparatus; (c) image of the pilot apparatus; light-off curves of 300 ppm (d) and 2500 ppm (e) toluene combustion.

that the 0.1Pd/FeCrAl catalyst shows excellent activity for toluene combustion and has promising performance for the industrial VOC catalytic combustion at medium and low concentrations even under high space velocity.[65] So, it is suitable for the removal of high-flux VOCs. Based on these results, we designed and established a pilot apparatus, as shown in Fig. 7c. At present, this apparatus is under construction, and it is expected to achieve better results.

4 Conclusions

A simple, general and effective strategy is proposed to prepare novel electrically heated monolithic Pt and Pd catalysts supported on an FeCrAl wire. Thermal treatment results in the formation of a well-adhered alumina coating on the metallic substrate. In addition, Pt and Pd NPs with sizes of 2 nm to 5 nm are highly dispersed on the alumina coating. Under low-current DC power, the catalysts achieve nearly 100% VOC combustion ratio with a combustion response time of less than 30 s. Furthermore, the catalysts exhibit 100% CO_2 selectivity and outstanding activity under high space velocity. Meanwhile, the optimized catalyst exhibits excellent stability and reusability after 700 min of use, and provides the following advantages: (1) requirement of small equipment, (2) high-efficiency energy utilization, (3) self-heating, (4) rapid response velocity, (5) excellent activity under high space velocity, and (6) good stability. Thus, our strategy will provide a new route for the preparation and new application prospect of environmental catalysts in the future.

Conflicts of interest

There are no conflicts to declare.

Acknowledgements

This work was supported by the Natural Science Foundation of China (NO. 21506194 and 21676255), the Natural Science Foundation of Zhejiang Province (NO. Y16B070011), and the Commission of Science and Technology of Zhejiang province (NO.2017C03007, 2017C33106).

Notes and references

1 F. N. Aguero, B. P. Barbero, L. Gambaro and L. E. Cadus, *Appl. Catal., B*, 2009, **91**, 108–112.
2 K. Everaert and J. Baeyens, *J. Hazard. Mater.*, 2004, **109**, 113–139.
3 S. Scire, S. Minico, C. Crisafulli, C. Satriano and A. Pistone, *Appl. Catal., B*, 2003, **40**, 43–49.
4 T. Y. Li, S. J. Chiang, B. J. Liaw and Y. Z. Chen, *Appl. Catal., B*, 2011, **103**, 143–148.
5 J. E. C. Lerner, T. Kohajda, M. E. Aguilar, L. A. Massolo, E. Y. Sanchez, A. A. Porta, P. Opitz, G. Wichmann, O. Herbarth and A. Mueller, *Environ. Sci. Pollut. Res.*, 2014, **21**, 9676–9688.
6 W. B. Li, J. X. Wang and H. Gong, *Catal. Today*, 2009, **148**, 81–87.
7 M. S. Kamal, S. A. Razzak and M. M. Hossain, *Atmos. Environ.*, 2016, **140**, 117–134.
8 Y. X. Liu, J. G. Deng, S. H. Xie, Z. W. Wang and H. X. Dai, *Chin. J. Catal.*, 2016, **37**, 1193–1205.
9 S. Wahid and B. J. Tatarchuk, *Ind. Eng. Chem. Res.*, 2013, **52**, 15494–15503.
10 L. F. Liotta, *Appl. Catal., B*, 2010, **100**, 403–412.
11 H. Li, Y. Wang, X. Chen, S. Liu, Y. Zhou, Q. L. Zhu, Y. F. Chen and H. F. Lu, *RSC Adv.*, 2018, **8**, 14806–14811.
12 S. Benard, M. Ousmane, L. Retailleau, A. Boreave, P. Vernoux and A. Giroir-Fendler, *Can. J. Civ. Eng.*, 2009, **36**, 1935–1945.
13 S. C. Kim and W. G. Shim, *Appl. Catal., B*, 2009, **92**, 429–436.
14 S. Scire and L. F. Liotta, *Appl. Catal., B*, 2012, **125**, 222–246.
15 H. F. Lu, Y. Zhou, W. F. Han, H. F. Huang and Y. F. Chen, *Catal. Sci. Technol.*, 2013, **3**, 1480–1484.
16 X. L. Weng, Q. J. Meng, J. J. Liu, W. Y. Jiang, S. Pattisson and Z. B. Wu, *Environ. Sci. Technol.*, 2019, **53**, 884–893.
17 P. F. Sun, W. L. Wang, X. L. Weng, X. X. Dai and Z. B. Wu, *Environ. Sci. Technol.*, 2018, **52**, 6438–6447.
18 X. L. Weng, P. F. Sun, Y. Long, Q. J. Meng and Z. B. Wu, *Environ. Sci. Technol.*, 2017, **51**, 8057–8066.
19 W. C. Hua, C. H. Zhang, Y. L. Guo, G. T. Chai, C. Wang, Y. Guo, L. Wang, Y. S. Wang and W. C. Zhan, *Appl. Catal., B*, 2019, **255**, 117748.
20 X. Zhang and D. Wu, *Ceram. Int.*, 2016, **42**, 16563–16570.
21 K. S. Yang, J. S. Choi and J. S. Chung, *Catal. Today*, 2014, **97**, 159–165.
22 L. Giani, C. Cristiani, G. Groppi and E. Tronconi, *Appl. Catal., B*, 2006, **62**, 121–131.
23 V. Meille, *Appl. Catal., A*, 2006, **315**, 1–17.
24 W. Fei, S. C. Kuiry and S. Seal, *Oxid. Met.*, 2004, **62**, 29–44.
25 N. Burgos, M. Paulis, M. M. Antxustegi and M. Montes, *Appl. Catal., B*, 2002, **38**, 251–258.
26 L. M. Martinez, O. Sanz, M. I. Dominguez, M. A. Centeno and J. A. Odriozola, *Chem. Eng. J.*, 2009, **148**, 191–200.
27 M. Valentini, G. Groppi, C. Cristiani, M. Levi, E. Tronconi and P. Forzatti, *Catal. Today*, 2001, **69**, 307–314.
28 Y. Matatov-Meytal and M. Sheintuch, *Appl. Catal., A*, 2002, **231**, 1–16.
29 C. Badini and F. Laurella, *Surf. Coat. Technol.*, 2001, **135**, 291–298.
30 C. Z. Wang, L. P. Han, Q. F. Zhang, Y. K. Li, G. F. Zhao, Y. Liu and Y. Lu, *Green Chem.*, 2015, **17**, 3762–3765.
31 O. Sanz, F. J. Echave, M. Sanchez, A. Monzon and M. Montes, *Appl. Catal., A*, 2008, **340**, 125–132.
32 H. Sun, X. Quan, S. Chen, H. Zhao and Y. Zhao, *Appl. Surf. Sci.*, 2007, **253**, 3303–3310.
33 S. Cimino, A. Gambirasi, L. Lisi, G. Mancino, M. Musiani, L. Vazquez-Gomez and E. Verlato, *Chem. Eng. J.*, 2016, **285**, 276–285.
34 Z. X. Zhang, Z. Jiang and W. F. Shangguan, *Catal. Today*, 2016, **264**, 270–278.
35 J. Yang, Y. Chen, L. Cao, Y. Guo and J. Jia, *Environ. Sci. Technol.*, 2016, **46**, 441–446.

36 F. N. Aguero, B. P. Barbero, L. C. Almeida, M. Montes and L. E. Cadus, *Chem. Eng. J.*, 2011, **166**, 218–223.
37 J. Lojewska, A. Kolodziej, J. Zak and J. Stoch, *Catal. Today*, 2005, **105**, 655–661.
38 O. Sanz, L. C. Almeida, J. M. Zamaro, M. A. Ulla, E. E. Miro and M. Montes, *Appl. Catal., B*, 2008, **78**, 166–175.
39 M. R. Morales, B. P. Barbero and L. E. Cadus, *Catal. Lett.*, 2011, **141**, 1598–1607.
40 Y. Diaz, A. Sevilla, A. Monaco, F. J. Mendez, P. Rosales, L. Garcia and J. L. Brito, *Fuel*, 2013, **110**, 235–248.
41 J. E. Samad, J. A. Nychka and N. V. Semagina, *Chem. Eng. J.*, 2011, **168**, 470–476.
42 B. P. Barbero, L. Costa-Almeida, O. Sanz, M. R. Moralesand, L. E. Cadus and M. Montes, *Chem. Eng. J.*, 2008, **139**, 430–435.
43 I. Yuranov, N. Dunand, L. Kiwi-Minsker and A. Renken, *Appl. Catal., B*, 2002, **36**, 183–191.
44 J. Dendooven, R. K. Ramachandran, E. Solano, M. Kurttepeli, L. Geerts, G. Heremans, J. Ronge, M. M. Minjauw, T. Dobbelaere, K. Devloo-Casier, J. A. Martens, A. Vantomme, S. Bals, G. Portale, A. Coati and C. Detavernier, *Nat. Commun.*, 2017, **8**, 1074.
45 L. Perez-Mirabet, E. Solano, F. Martinez-Julian, R. Guzman, J. Arbiol, T. Puig, X. Obradors, A. Pomar, R. Yanez, J. Ros and S. Ricart, *Mater. Res. Bull.*, 2013, **48**, 966–972.
46 W. Wang, L. Zhuang, Y. Zhang and H. Shen, *Mater. Res. Bull.*, 2015, **69**, 61–64.
47 P. F. Hou, H. Liu, J. L. Li and J. Yang, *CrystEngComm*, 2015, **17**, 1826–1832.
48 S. Cimino, R. Gerbasi, L. Lisi, G. Mancino, M. Musiani, L. Vazquez-Gomez and E. Verlato, *Chem. Eng. J.*, 2013, **230**, 422–431.
49 P. Avila, M. Montes and E. E. Miro, *Chem. Eng. J.*, 2005, **109**, 11–36.
50 S. Zhao, J. Zhang, D. Weng and X. Wu, *Surf. Coat. Technol.*, 2003, **167**, 97–105.
51 J. A. Zamaro, M. A. Ulla and E. E. Miro, *Appl. Catal., A*, 2006, **308**, 161–171.
52 J. S. Jia, J. Zhou, H. U. Zhang, Z. S. Yuan and S. D. Wang, *Appl. Surf. Sci.*, 2007, **253**, 9099–9104.
53 J. Ma, Y. Lou, Y. F. Cai, Z. Y. Zhao, L. Wang, W. C. Zhan, Y. L. Guo and Y. Guo, *Catal. Sci. Technol.*, 2018, **8**, 2567–2577.
54 C. J. Powell, *J. Electron Spectrosc. Relat. Phenom.*, 2012, **185**, 1–3.
55 S. F. Song, Y. J. Wu, S. S. Ge, L. Wang, Y. L. Guo, W. C. Zhan and Y. Guo, *ACS Catal.*, 2019, **9**, 6177–6187.
56 S. D. Jackson, J. Willis, G. D. Mclellan, G. Webb, M. B. T. Keegan, R. B. Moyes, S. Simpson, P. B. Wells and R. Whyman, *J. Catal.*, 1993, **139**, 191–206.
57 L. Y. Lin and H. L. Bai, *Chem. Eng. J.*, 2016, **291**, 94–105.
58 H. B. Huang, Y. Xu, Q. Y. Feng and D. Y. C. Leung, *Catal. Sci. Technol.*, 2015, **5**, 2649–2669.
59 S. S. T. Bastos, S. A. C. Carabineiro, J. J. M. Orfao, M. F. R. Pereira, J. J. Delgado and J. L. Figueiredo, *Catal. Today*, 2012, **180**, 148–154.
60 D. Delimaris and T. Ioannides, *Appl. Catal., B*, 2009, **89**, 295–302.
61 P. Papaefthimiou, T. Ioannides and X. E. Verykios, *Appl. Catal., B*, 1997, **13**, 175–184.
62 J. E. Sawyer and M. A. Abraham, *Ind. Eng. Chem. Res.*, 1994, **33**, 2084–2089.
63 C. W. Ahn, Y. W. You, I. Heo, J. S. Hong, J. K. Jeon, Y. D. Ko, Y. Kim, H. Park and J. K. Suh, *J. Ind. Eng. Chem.*, 2017, **47**, 439–445.
64 H. Wang, W. Yang, P. H. Tian, J. Zhou, R. Tang and S. J. Wu, *Appl. Catal., A*, 2017, **529**, 60–67.
65 P. Zhang, H. Lu, Y. Zhou, L. Zhang, Z. Wu, S. Yang, H. Shi, Q. Zhu, Y. Chen and S. Dai, *Nat. Commun.*, 2015, **6**, 8446.

